



Rapid Fault Detection for Exhibition Light Box Groups Using PCI Bus Structure

Gong Chen^{*}, Sijie Wang, Haoran Tao, Qiyang Shen, Dandan Huang, Jiani Chen, Boyan Zheng, Zhengjie Jiang, Rui Shi, Luobing Xu, Yanmin Chen

College of Electrical and Information Engineering, Changzhou Institute of Technology, 213000 Changzhou, China

* Correspondence: Gong Chen (realchengong@sina.com)

Received: 08-15-2024

Revised: 09-18-2024

Accepted: 09-24-2024

Citation: G. Chen, S. J. Wang, H. R. Tao, Q. Y. Shen, D. D. Huang, J. N. Chen, B. Y. Zheng, Z. J. Jiang, R. Shi, L. B. Xu, and Y. M. Chen, "Rapid fault detection for exhibition light box groups using PCI bus structure," *J. Ind Intell.*, vol. 2, no. 3, pp. 189–200, 2024. <https://doi.org/10.56578/jii020305>.



© 2024 by the author(s). Published by Acadlore Publishing Services Limited, Hong Kong. This article is available for free download and can be reused and cited, provided that the original published version is credited, under the CC BY 4.0 license.

Abstract: The internal translucent color light box serves as both a display and behavioral guidance tool in exhibitions. However, its functionality can be compromised by variations in light intensity, temperature, humidity, bolt fastening integrity, and door lock status. Conventional Internet of Things (IoT)-based systems, while effective, often involve the installation of expensive sensors, control units, and network infrastructure within each light box. Given the large number of light boxes typically used in exhibitions, the high cost and slow response time of such systems remain significant limitations. This study proposes a novel approach utilizing a Peripheral Component Interconnect (PCI) bus structure to form a network of interconnected light boxes. By sequentially collecting voltage and current data from photosensitive resistors across adjacent groups of four light boxes, faults can be rapidly identified through a hierarchical comparison method. This method enables precise fault localization with minimal cost and at significantly reduced time. Simulations and physical prototypes were developed using Multisim to model the changes in light intensity during the fault detection process. Experimental results demonstrate the system's ability to accurately pinpoint malfunctioning light boxes when light levels fall below 1000 lx. The detection accuracy reaches 100% under these conditions. Notably, the proposed system requires no complex control processing, and offers an over 90% reduction in detection time and cost compared to traditional manual inspections and IoT-based fault detection systems. This approach presents a highly cost-effective and efficient solution for exhibition light box fault localization, facilitating maintenance by enabling visual identification of malfunctioning units.

Keywords: PCI bus structure; Fault detection; Photosensitive resistance; Positioning

1 Introduction

China's 14th Five-Year Plan and Vision 2035 Outline highlight the imperative to strengthen the application of key digital technology innovation, focusing on key algorithms, sensors and other key areas of artificial intelligence (AI). The advertising display technology based on AI and the IoT is one of the key aspects of China's key digital technology innovation. However, in practical application, the traditional light box group is simple to make, small in size and low in cost, and is not suitable for online monitoring of light intensity, temperature and humidity, bolt fastening, door lock closure and other working conditions inside the light box. At the same time, the traditional IoT technology requires multiple groups of light boxes using multiple sensors and network modules, resulting in high costs and difficult control costs.

At present, domestic and foreign researchers have done relatively in-depth theoretical, experimental and simulation research on the light box control and light-emitting diode (LED) light sources. Zhang [1] proposed an advertising light box remote monitoring device, which includes a light status acquisition module, an ambient light status acquisition module, a remote light control module, a timed light control module, a central control module and a wireless communication module. In addition, the signal outputs of the light status acquisition module and the ambient light status acquisition module are connected to the signal input of the central control module. The cost of this method is too high and the demand for wireless modules is too large. Shi [2] proposed an IoT human-computer interaction to self-check the light source carrier. The LED backlight is driven by a driver. The microcontroller unit (MCU) processor is the core component, which is connected to the LED backlight detection module, the box

door closure detection module, the screw loosening detection module, and the urban IoT module, and is used for information acquisition and processing. The LoRa module is connected to the MCU processor for transmitting the wireless information, which is sent to the gateway, and then transmitted to the mobile terminal, which includes the cell phone and the computer, and has the software for information display. The mobile terminal has software or an app for information display. However, the detection modules used include photosensitive, voltage, and current, which have high costs. Zhu et al. [3] introduced a solar energy automatic control advertising light box system with a fault indication and remote fault alarm function, which can automatically adjust the lighting to full or half intensity according to the need, but the response time is too long, which is not conducive to the rapid positioning of the exhibition light box. The studies [4–8] mainly focused on light intensity improvement for the design of light box size and light source and came up with the optimal LED arrangement to extend the life of the LED light source in the light box. Jin and Wu [9] studied the centralized power supply mode and standby lamp mode to reduce EMI interference and improve energy saving effect. Xiong et al. [10] proposed a network environment based on the LED by using the WiFi module ESP8266 as a wireless communication for data transmission, thus realizing the ULN2987 chip for the LED lighting system drive and its control of the lighting system. However, the LED damage can not be detected and located. Zhejiang Lingqi Optoelectronics Technology Co., Ltd. set up an IoT communication module in each light box and self-organized the local area network to enable the light box to be combined into a huge IoT system. The studies [11–19] assessed the colour quality of LED sources, such as naturalness, attractiveness, and difference and also focused on color preference, color rendition, color rendering and conference on mechanical. The study [20] focused on solving color reproducibility between digital devices, warm white LEDs and solutions to the cyan gap in the full-spectrum W-LED lighting. The study [21] introduced an LED light propagation cavity and LED-based Fourier transform absorption spectroscopy. The study [22] studied the effects of stage lighting and developed a public lighting system with smart lighting control systems. It is no doubt that this contributes to the LED program. The system enables real-time connectivity with cloud platforms via wired networks, 4G network cards, or existing wireless networks. In addition, fault detection within the circuit system can be achieved, along with the integration of various external sensor devices for environmental monitoring, human flow monitoring, bolt fastening status monitoring, and door lock closure status monitoring.

2 Fast Fault Detection Model

2.1 PCI Bus Structure Model

The PCI bus is a tree structure, which can be connected to PCI devices and bridges. The PCI bus only allows a PCI master device, and the other ones are PCI slave devices. Read and write operations can only be performed between master and slave devices, and data exchange between slave devices needs to be relayed through the master device.

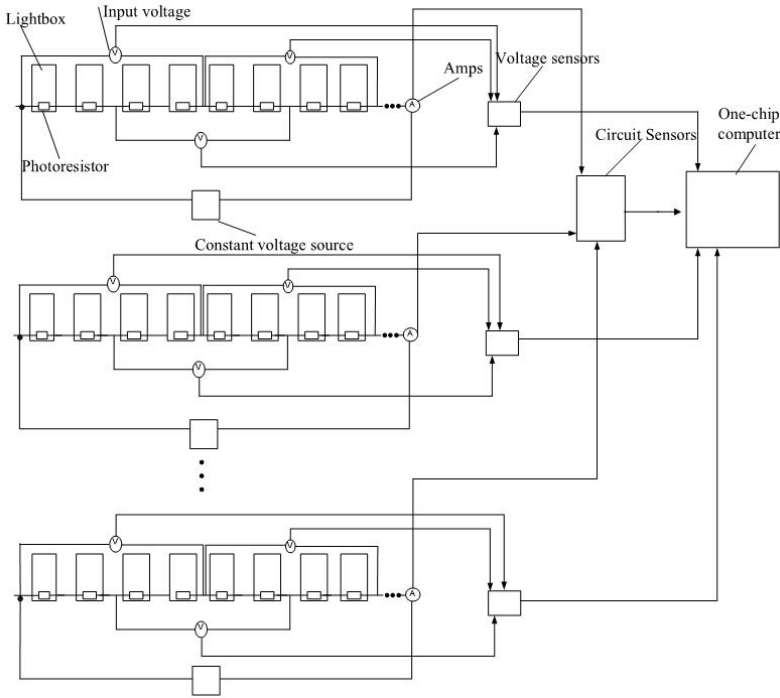


Figure 1. Working principle diagram of the PCI bus structure

This study imitates the PCI bus structure model. The number of six times the number of light box group photoresistors (in order to avoid breakage; two photoresistors can be used in parallel) in series was used inside the constant voltage circuit, with the failure of the light box group as the master device and the normal working group as the first slave device. Current sensors were set up in the first slave device, with every four light boxes in series with a voltage sensor and separated by two light boxes. Analogous to the first slave device, a current sensor was set up in the first slave device. N slave devices were built similar to the first slave device. The current and voltage sensor data of each master and slave device were summarized through the Input/Output (IO) port of the microcontroller, and were then output to the cloud through the wireless WiFi module. The microcontroller and WiFi module are similar to the trunk of the tree, while the serial branches are similar to the branches, which is the overall tree structure.

The specific working principle diagram is shown in Figure 1, which contains the photosensitive resistor, the voltage sensor V, the current sensor A, the light box, the voltage data acquisition device, the current data acquisition device, and the microcontroller to complete the fault detection work.

As shown in Figure 1, when the light box fails, the light inside the light box becomes weak and the resistance value of the photosensitive resistor changes, resulting in the increases of local resistance, thus affecting the current and voltage changes. Therefore, the current and voltage sensors, positioned to detect these variations, transmit the acquired signals to the microcontroller for data processing. The processed data are then transmitted to the receiving terminal via the WiFi device, enabling the precise identification of the failure location of the light box.

2.2 Determining the Failure of a Light Box Within a String Light Box Group

The specific fault detection schematic diagram is shown in Figure 2. Let the voltage sensor measurement values of the first string of light boxes are represented by $V_{11}, V_{12}, \dots, V_{1(P-1)}$, and V_{1P} , respectively. V_{11} measures four light boxes, spaced with two light boxes apart. V_{12} measures four light boxes, spaced with two light boxes apart. This is the abbreviated 4-2-4 pattern. The voltage sensor measurements for the second string of light boxes are represented by $V_{21}, V_{22}, \dots, V_{2(P-1)}$, and V_{2P} , respectively. The measured values of the voltage sensors for the n -th string of light boxes are represented by $V_{n1}, V_{n2}, \dots, V_{n(P-1)}$, and V_{nP} , respectively.

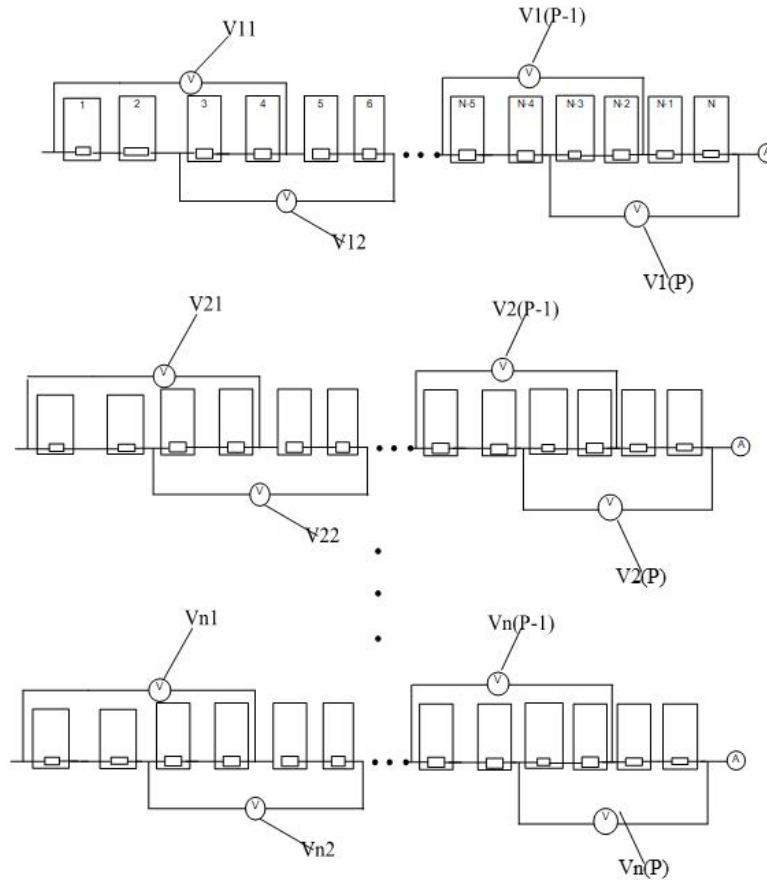


Figure 2. Principle analysis diagram

A string of light box current sensors is within the normal current range of $a \leq I \leq b$. If the current is not in the

range, then a string of light boxes within the group or a number of faults (usually one fault) should be determined. Assuming that only one light box fails, the faulty string light box group is the i -th string.

When the array of a string of light boxes becomes dim in terms of its light level, the voltage sensor measurement values of this string of light boxes and other light boxes are different. Through the analysis of these deviation values, the location of the fault of a light box within a string light box group can be determined.

(a) If $V_{i1} > V_{j1}$, and $V_{i2} < V_{j2}$, where $j(j = i + 1; \text{ or } j = i - 1)$ is a non-faulty light box string adjacent to the faulty light box group string and $j \neq i$, then a fault occurs in the 1st and 2nd light boxes in the i -th string;

(b) If $V_{i1} > V_{j1}$, and $V_{i2} > V_{j2}$, where j is a non-faulty light box string adjacent to the faulty light string and $j \neq i$, then a fault occurs in the 3rd and 4th light boxes in the i -th string;

(c) If $V_{i1} < V_{j1}$, and $V_{i2} > V_{j2}$, where j is a non-faulty light box string adjacent to the faulty light group string and $j \neq i$, then a fault occurs in the 5th and 6th light boxes in the i -th string;

(d) If $V_{i2} < V_{j2}$, and $V_{i1} < V_{j1}$, where j is the faulty lamp group string adjacent to the non-faulty lamp box string and $j \neq i$, then the lamp box measured by the voltage sensor in the i -th string is not faulty, and the fault is in this lamp box string;

(e) If $V_{i3} > V_{j3}$, and $V_{i4} < V_{j4}$, where j is a non-faulty light box string adjacent to the faulty light group string and $j \neq i$, then a fault occurs in the 7th and 8th light boxes in the i -th string;

(f) If $V_{i3} > V_{j1}$, and $V_{i4} > V_{j2}$, where j is a non-faulty light box string adjacent to the faulty light group string and $j \neq i$, then a fault occurs in the 9th and 10th light boxes in the i -th string;

(g) If $V_{i3} < V_{j1}$, and $V_{i4} > V_{j2}$, where j is a non-faulty light box string adjacent to the faulty light group string and $j \neq i$, then a fault occurs in the 11th and 12th light boxes in string i ;

(h) If $V_{i3} < V_{j1}$, and $V_{i4} < V_{j2}$, where j is a non-faulty light box string adjacent to the faulty light group string and $j \neq i$, then the light box measured by the voltage sensor in the i -th string is not faulty and the fault is in this light box string.

Following the above analysis and judgment, the n -th light box also applies.

2.3 Validation of the Analysis Process

As shown in the Figures 3 and 4, it is known that the power supply of each closed circuit is U . Each light box has the same value of resistance, and the photoresistor increases as the light decreases in resistance. Figure 3 shows the faulty group and Figure 4 shows the normal control group.

If $RI1$ perceives a decrease in illumination, it is known that its resistance value increases.

If $U_{11} = \frac{RI1+RI2}{RI1+RI2+RI3+RI4}U$, then U_{11} increases;

If $U_{21} = \frac{RJ1+RJ2}{RJ1+RJ2+RJ3+RJ4}U$, then U_{21} is unchanged;

If $U_{12} = \frac{RI2+RI3}{RI1+RI2+RI3+RI4}U$, then U_{12} decreases;

If $U_{22} = \frac{RJ2+RJ3}{RJ1+RJ2+RJ3+RJ4}U$, then U_{22} is unchanged.

From the above equations, it can be seen that when no failure occurs, $U_{11} = U_{21} = U_{12} = U_{22}$. If $RI1$ fails, then $U_{11} > U_{21}$ and $U_{12} < U_{22}$. If $RI2$ fails, then $U_{11} > U_{21}$ and $U_{12} > U_{22}$. If $RI3$ fails, then $U_{11} < U_{21}$ and $U_{12} > U_{22}$. If $RI4$ fails, then $U_{11} < U_{21}$ and $U_{12} < U_{22}$.

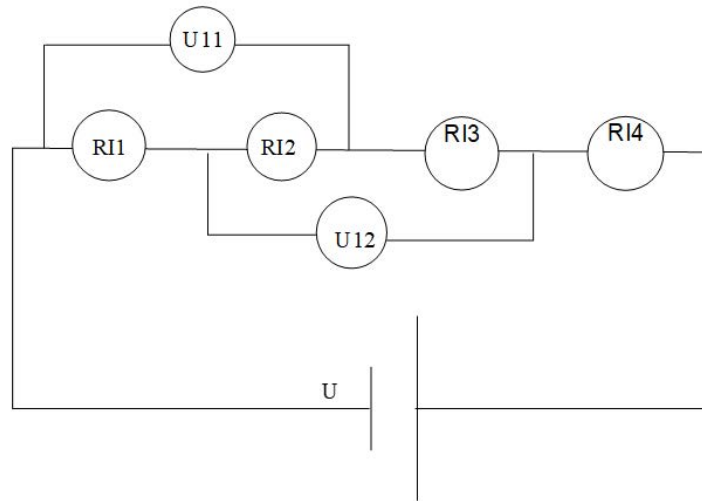


Figure 3. Faulty light box group

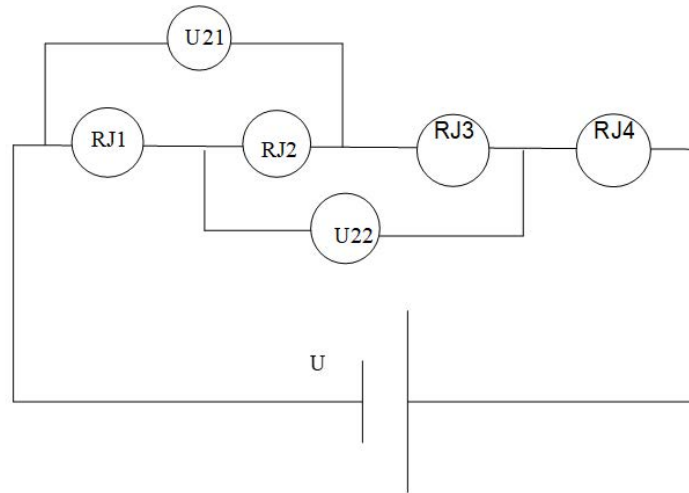


Figure 4. Normal control light box group

3 Modeling Simulation and Analysis Using Multisim

As shown in Figure 5, in order to simulate the decline in illumination, the resistance values of $R1$, $R3$ and $R5$ resistors were increased in the first row of the faulty group and the resistance value of each resistor was kept constant in the second row of the normal working group. Figure 6 shows a comparison of the output current and voltage of the faulty and normal string groups, and the trend of both voltage and current is basically the same when the three resistors in different positions are changed. Taking subgraphs (a)-(c) of Figure 6 as an example, when $R1$ is changed, $U_{21} = U_{22} = 3.33$ V is the voltage of the normal working string group and $49.02 \mu\text{A}$ is the current of the normal working string group. In the case of the faulty string group, the initial resistance is set at $17 \text{ K}\Omega$, and the fault resistance of the analog photoresistor is required to exceed this value ($17 \text{ K}\Omega$). At this time, the faulty string current is less than $49.02 \mu\text{A}$, and $U_{11} > U_{21}$ and $U_{12} < U_{22}$, consistent with the theoretical analysis.

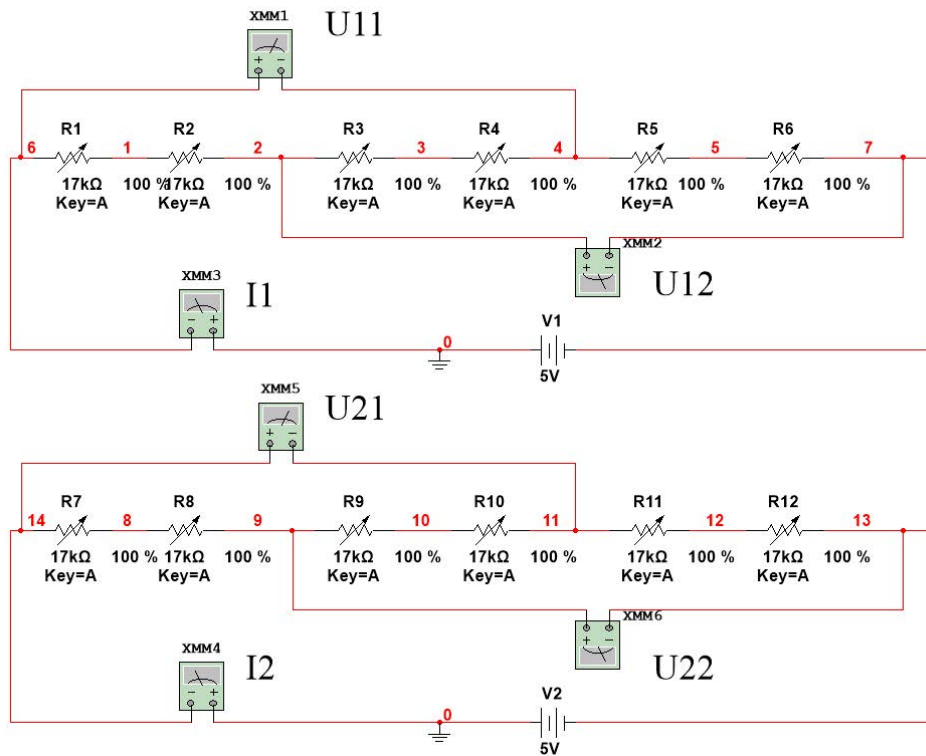
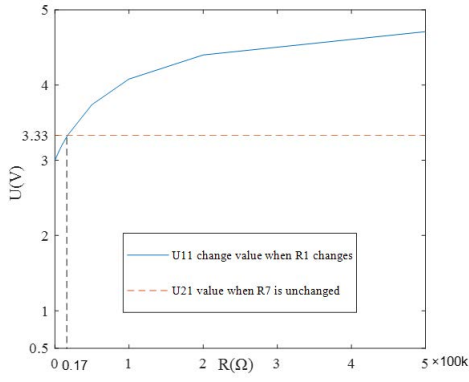
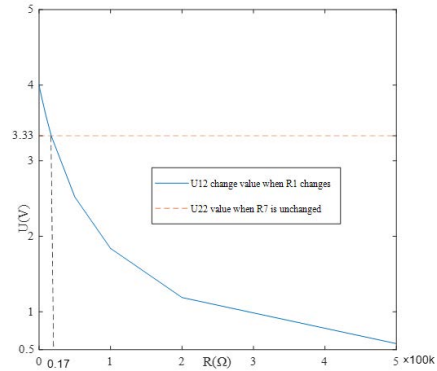


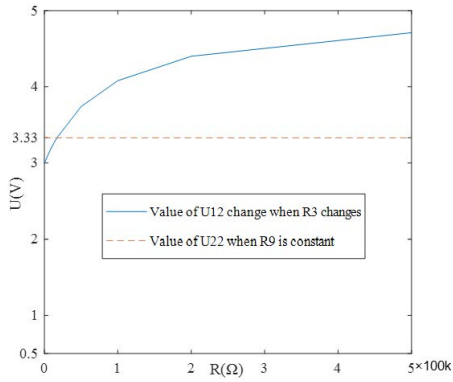
Figure 5. Photoresistor analog Multisim simulation diagrams



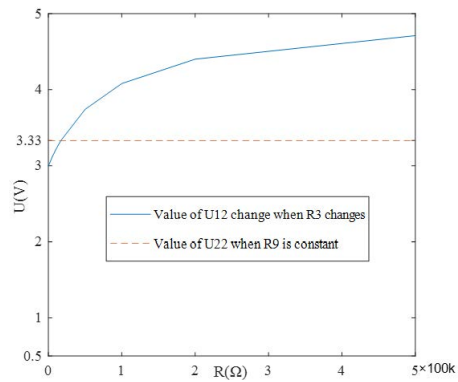
(a)



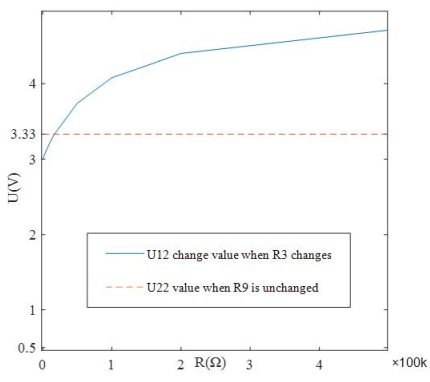
(b)



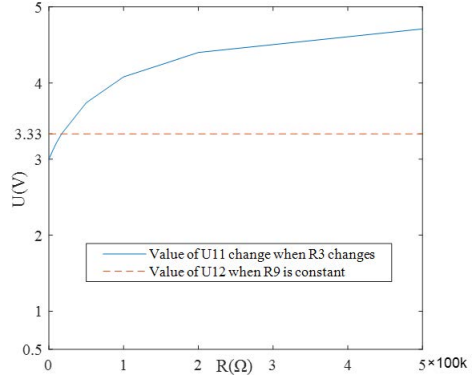
(c)



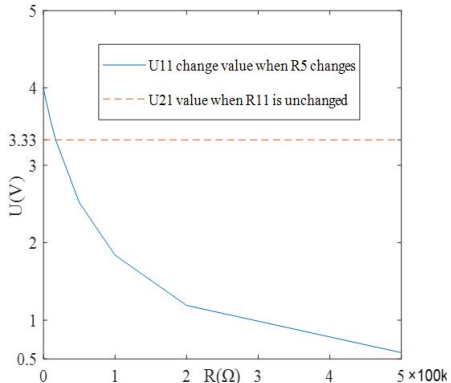
(d)



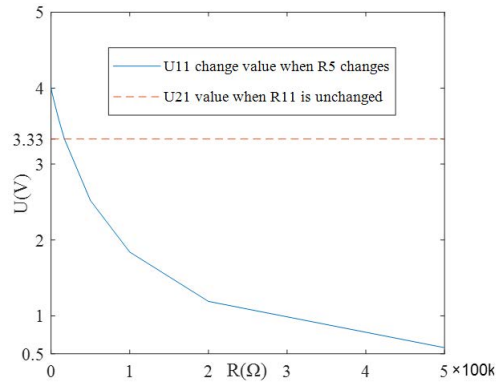
(e)



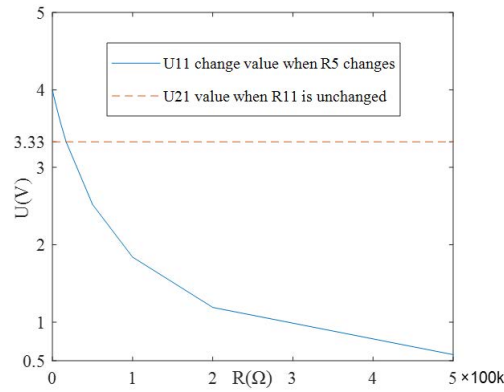
(f)



(g)



(h)



(i)

Figure 6. Comparison of output parameters along with changes in resistor resistance at different positions under simulation conditions: (a) U11 change value when R1 changes and U21 value when R7 is unchanged; (b) U12 change value when R1 changes and U22 value when R7 is unchanged; (c) Value of U12 change when R3 changes and Value of U22 when R9 is constant; (d) U11 change value when R3 changes and U21 value when R9 is unchanged; (e) U12 change value when R3 changes and U22 value when R9 is unchanged; (f) Value of U11 change when R3 changes and Value of U12 when R9 is constant; (g) U11 change value when R5 changes and U21 value when R11 is unchanged; (h) U11 change value when R5 changes and U21 value when R11 is unchanged; (i) U11 change value when R5 changes and U21 value when R11 is unchanged

4 Platform Construction and Test Analysis

A test platform was built, as shown in Figure 7, incorporating a control box switching power supply (220 V AC input, 24 V and 5V DC output) and an STM32 microcontroller, which is connected to 18 A4-sized light boxes according to the PCI bus structure. Each set of six light boxes is connected in series with a 5 V supply, with the first row designated as the faulty string group and the remaining two rows as the normal working string group. In accordance with the simulation settings, each string group was equipped with two voltage sensors, connected to the microcontroller's IO port via Analog-to-Digital (AD) sampling. A total of six samples were collected from the three string groups. Below the light boxes, a photoresistor (GL5506, resistance range of 2 kΩ to 2000 kΩ) was installed. A signal isolator, operating with a DC voltage of 24 V and an input current range of 0-0.62 A DC, was used to convert the current from the three series branches into a corresponding voltage output. The software for the system was developed using Windows Forms.

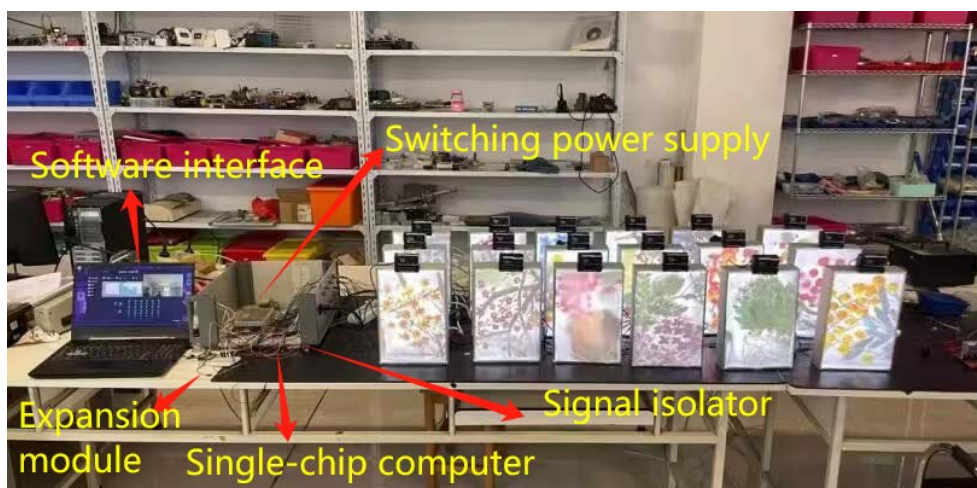


Figure 7. Rapid inspection platform based on the PCI bus structure with light box cluster

In Figure 7, the simulated faults were selected in the same way as the simulation. That is, the first row was selected as the faulty working group, which simulates the change of light intensity by blocking the eight LED beads in the light box in turn. The second row was selected as the normal working group. The light intensity (I_x) in different cases was collected using an illuminance meter, and the current and voltage values were collected sequentially.

Taking subgraphs (a)-(c) of Figure 8 as an example, 3.03 V is the voltage of the normal working string group, and 24 mv is the transformed value of the normal working string current through the signal isolator. The measured results are basically consistent with the simulation trend.

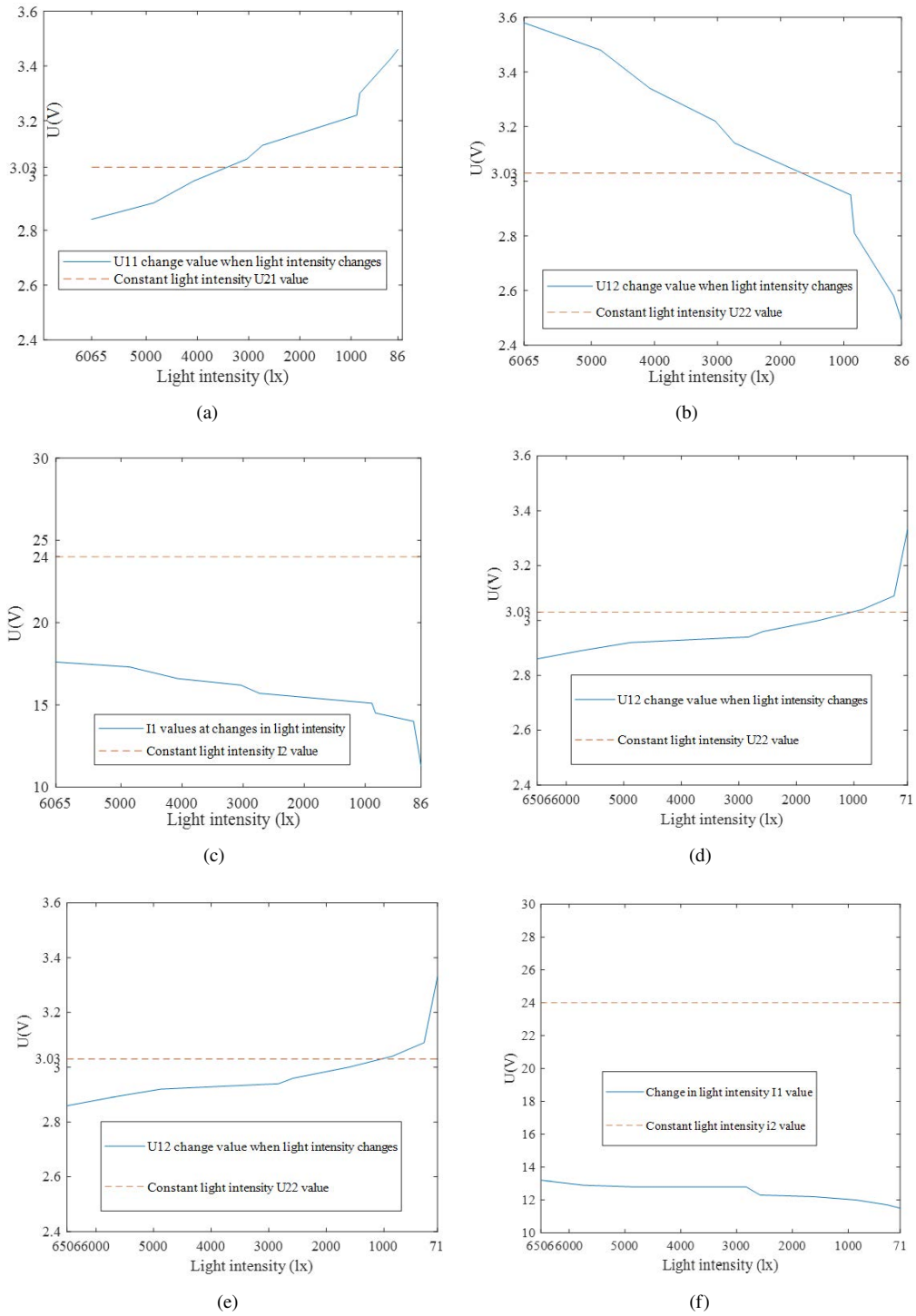


Figure 8. Output data diagram when the resistance values of different positions change under measured conditions: (a) U11 change value when light intensity changes and constant light intensity U21 value; (b) U12 change value when light intensity changes and constant light intensity U22 value; (c) I1 values at changes in light intensity and constant light intensity I2 value; (d) U12 change value when light intensity changes and constant light intensity U22 value; (e) U12 change value when light intensity changes and constant light intensity U22 value; (f) Change in light intensity I1 value and constant light intensity i2 value

As shown in Table 1, the first row of the first light box gives the faulty light box voltage and current conversion

values under different masking conditions. With the increase in the number of blocking lamp beads, the photoresistor resistance increases and the light intensity in the light box decreases. The output voltage values of the first four light boxes in the first row gradually increase, whereas the output voltage values of the two light boxes apart decrease. The voltage value of the series circuit current converted by the isolator decreases. As long as the lamp beads are blocked, the circuit current is significantly smaller than the working group, which is consistent with the theory.

Table 1. Measurement data of the faulty light box under different shading conditions

Masking Number of Lamp Beads (pcs)	1	2	3	4	5	6	7	8	Turning Off the Power
U11 (V)	2.84	2.9	2.98	3.06	3.11	3.22	3.3	3.43	3.46
U12 (V)	3.58	3.48	3.34	3.22	3.14	2.95	2.81	2.58	2.49
Current conversion value (mV)	17.6	17.3	16.6	16.2	15.7	15.1	14.5	14	11.3
Light intensity (lx)	6065	4854	4071	3036	2732	891.4	832	209.3	86

When the light intensity is lower than 1000 lx, the detection accuracy of the experiment reaches 100%. When the number of blocked LEDs is seven, the fault string voltage U_{11} (3.3 V) is greater than the normal group voltage U_{21} (3.03 V) and the fault string voltage U_{12} (2.81 V) is less than the normal group voltage U_{22} (3.03 V), which are all in line with theoretical analysis. When the number of blocked LEDs is less than six, such as five, the fault string voltage U_{11} (3.11 V) is greater than the normal group voltage U_{21} (3.03 V) and the fault string voltage U_{12} (3.14 V) is greater than the normal group voltage U_{22} (3.03 V). At this time, the judgment result does not conform to the theoretical analysis. The main reason is that the data acquisition circuit has internal resistance. Under low light conditions, the resistance value change range of the photoresistor is similar to the error range caused by the internal resistance, resulting in data acquisition deviation. In addition, the photoresistor used in the research has a low sensitivity, and the resistance value of the photoresistor is not linearly related to the light intensity, making it difficult to accurately capture small changes.

Table 2 shows the detection results under different fault types and the response time of the PCI bus structure in handling different fault situations.

Table 2. Detection data of different fault types

Fault Type	Number of Blocking Lamp Beads (pes)	U11 (V)	U12 (V)	Current Conversion Value (mV)	Light Intensity (lx)	Response Time (ms)
Short-circuit fault	1	1.53	1.61	25.1	6071	2.8
	2	1.49	1.63	24.6	4856	2.9
	3	1.54	1.59	24	4075	3
	4	1.57	1.68	23.5	3038	3.2
	5	1.62	1.72	23	2730	3.3
	6	1.66	1.75	22.4	892	3.4
	7	1.64	1.78	21.9	835	3.5
	8	1.69	1.8	21.5	211	3.6
Overload fault	1	1.82	2.08	22.3	6073	4
	2	1.85	2.12	21.8	4858	4.2
	3	1.89	2.15	21.4	4073	4.4
	4	1.91	2.18	21	3039	4.6
	5	1.87	2.21	20.6	2729	4.8
	6	1.93	2.23	20.2	895	5
	7	1.9	2.26	19.8	839	5.2
	8	1.95	2.29	19.4	208	5.4

In order to compare with the traditional detection methods, the following scene (an area of 3 m × 6 m in Figure 9) was set and the failure of 18 light boxes was simulated in turn.

The light boxes were arranged into a 3 × 6 array, with a spacing of 1 m. Inspection simulations were initiated at a distance of 2 m from the light boxes, with the inspectors walking at a speed of 80 cm/s. As shown in Table 3, the inspection time for the 18 m² area ranges from 2 s to 8 s.

Table 4 shows the comparison of indicators of different testing methods. It can be observed that the indicators of the proposed method and the traditional IoT technology are significantly better than those of manual inspection. In

particular, the detection time is improved from seconds to milliseconds, reflecting the high efficiency of automation instead of manual labor. In addition, compared to the traditional IoT technology, the detection time of the proposed method is determined by the hardware response time. Therefore, the difference is not significant. However, if it involves a large area of use of the light box group, the number of hardware used in this scheme is fewer and the detection time is shorter than the traditional IoT technology. In terms of the price and number of considerations, the cost of sensors in the perception layer is reduced by 95%. The cost of the wireless module is reduced by 94%.



Figure 9. Simulation of the convention light box arrangement

Table 3. Manual inspection time of the faulty light box

Light Box Serial Number	Time (s)	Light Box Serial Number	Time (s)
1	7.4	10	4.4
2	6.7	11	3.2
3	5.9	12	2.4
4	4.2	13	7.4
5	3.6	14	6.4
6	2.5	15	5.4
7	7.1	16	4.8
8	6.5	17	3.5
9	5.5	18	2.9

Table 4. Comparison of indicators of different testing methods

Detection Methods	Detection Time	Costs
Manual inspection	$2\text{ s} < t < 8\text{ s}$ (an area of $3\text{ m} \times 6\text{ m}$)	(1) Lightness sensor: $10\text{ yuan} / \text{a} \times 18 = 180\text{ yuan}$ (2) Labor inspection cost: $200\text{ yuan} / \text{day}$
Traditional IoT with each light box having wireless WiFi	$< 5\text{ ms}$	(1) Illuminance sensor: $10\text{ yuan} / \text{a} \times 18 = 180\text{ yuan}$ (2) Wireless WiFi: $8\text{ yuan} / \text{a} \times 18 = 164\text{ yuan}$
The proposed method	$< 4\text{ ms}$	(1) Photoresistor: $0.5\text{ yuan} / \text{a} \times 18 = 9\text{ yuan}$ (2) Wireless WiFi: $8\text{ yuan} / \text{a} \times 1 = 8\text{ yuan}$

5 Discussion

The number of convention and exhibition display light boxes often exceeds one hundred. In the traditional method, one light box is equipped with a sensor, combined with wireless WiFi or wired module networking. The main problem is that the sensor is costly for the digital output though it is highly precise and the corresponding time is slow. In addition, a light box equipped with a network module also has the problem of high costs. The working state detection of the light box for exhibition does not need high precision, and the cost requirement is also high. Using the PCI bus structure to form a group of light box programs, the sensor is a low-cost resistor and more than ten light boxes only need a microcontroller and a network module. This setup not only significantly reduces costs but also enables fast data collection via analog signal outputs from the microcontroller, which fully meets the moderate precision requirements for exhibition lighting. The program test results show that the illumination is less than 1000 lx when the detection accuracy is 100%. And the detection time and the cost are lower than the traditional detection methods. In actual use, in order to prevent the work failure of the whole string of light box groups caused by multiple series-connected photoresistor breakage, two photoresistors can be used in parallel in the light box to avoid the occurrence of the above situation.

6 Conclusions

The light box group fault detection technology based on the PCI bus structure is suitable for large-scale light box exhibition activities. For exhibitions with a limited budget, the traditional method is highly dependent on hardware, and it is difficult to support its high cost. This study provides an economic and cost-effective method, which can reduce hardware input as much as possible with low cost and easier ways of promotion. At the same time, the research method is simple in design and compact in structure, which is more suitable for short-term exhibition with limited time, and is easy to detect and determine the fault of the light box, which improves the maintenance efficiency. Although the proposed method has the advantage of low cost and high portability, it still faces challenges and limitations. Due to the limitation of cost, the sensitive resistor used in the research has low precision and is limited in the demand of high-precision scenarios. In the future, it could be optimized under the constraint of cost to appropriately improve the detection accuracy. In addition, under the condition of light intensity below 1000 lx, the detection accuracy is as high as 100%. But under high light intensity, there are still errors and the accuracy is reduced. Because of the characteristics of the photoresistor, this technology is easy to disturb in the environment of strong changes in light. This technology has a wide application prospect in practical applications, but it still needs to be optimized to improve the accuracy and adaptive ability.

Data Availability

The data used to support the research findings are available from the corresponding author upon request.

Conflicts of Interest

The authors declare no conflict of interest.

References

- [1] K. Zhang, "A remote monitoring device for advertising light box lighting," Tianjin: CN205507478U, 2016.
- [2] B. Shi, "A light source carrier for human-computer interaction and self checking in the Internet of Things," Zhejiang: CN207235168U, 2018.
- [3] Q. Y. Zhu, C. L. Wen, W. Y. Xie, J. J. Ye, and H. Yin, "Solar energy automatically controlled advertising light box system," *Appl. Mech. Mater.*, vol. 148-149, pp. 101–105, 2011. <https://doi.org/10.4028/www.scientific.net/amm.148-149.101>
- [4] T. Lei, "Led advertising light box lighting design," *Electron. World*, vol. 2021, no. 4, pp. 134–135, 2021. <https://doi.org/10.19353/j.cnki.dzsj.2021.04.061>
- [5] C. Tsuei, W. Sun, and C. Kuo, "Hybrid sunlight/LED illumination and renewable solar energy saving concepts for indoor lighting," *Opt. Express*, vol. 18, no. S4, p. A640, 2010. <https://doi.org/10.1364/oe.18.00a640>
- [6] Y. Li, "Study on the visual recognition of white chinese character identification in translucent color light box," *Chongqing Univ.*, 2021. <https://doi.org/10.27670/d.cnki.gcqdu.2021.000245>
- [7] F. Wu, H. Xu, F. Rao, Y. Sun, X. Zhang, and Y. Zhang, "Design of large format high brightness LED light guide board light box," *China Light. Soc.*, p. 7, 2017. <https://doi.org/10.3969/j.issn.1002-6150.2017.12.002>
- [8] M. Li, "Multi-functional new type light box advertisement for power saving at bus stations," *Sci. Technol. Innov. Appl.*, vol. 2016, no. 36, pp. 14–15, 2016. <https://doi.org/10.19981/j.cn23-1581/g3.2016.35.009>
- [9] Y. Jin and J. Wu, "Research on intelligent advertising light box groups with centralized power supply mode," *J. Dalian Univ.*, vol. 2006, no. 2, pp. 50–55, 2006. <https://doi.org/10.3969/j.issn.1008-2395.2006.02.013>

- [10] Q. Xiong, L. Li, Z. Qi, H. Liang, W. Xu, and W. Zeng, "Design and implementation of a simple LED lighting system based on WiFi environment," *Electron. Meas. Technol.*, vol. 40, no. 8, pp. 231–234, 2017. <https://doi.org/10.19651/j.cnki.emt.2017.08.051>
- [11] S. Jost-Boissard, P. Avouac, and M. Fontoynt, "Assessing the colour quality of LED sources: Naturalness, attractiveness, colourfulness and colour difference," *Light. Res. Technol.*, vol. 47, no. 7, pp. 769–794, 2014. <https://doi.org/10.1177/1477153514555882>
- [12] M. Wei, K. W. Houser, G. R. Allen, and W. W. Beers, "Color preference under LEDs with diminished yellow emission," *LEUKOS*, vol. 10, no. 3, pp. 119–131, 2014. <https://doi.org/10.1080/15502724.2013.865212>
- [13] K. W. Houser, M. Wei, A. David, M. R. Krames, and X. S. Shen, "Review of measures for light-source color rendition and considerations for a two-measure system for characterizing color rendition," *Opt. Express*, vol. 21, no. 8, p. 10393, 2013. <https://doi.org/10.1364/oe.21.010393>
- [14] M. S. Rea and J. P. FreyssinierNova, "Color rendering: A tale of two metrics," *Color Res. Appl.*, vol. 33, no. 3, pp. 192–202, 2008. <https://doi.org/10.1002/col.20399>
- [15] K. A. G. Smet and P. Hanselaer, "Impact of cross-regional differences on color rendition evaluation of white light sources," *Opt. Express*, vol. 23, no. 23, p. 30216, 2015. <https://doi.org/10.1364/oe.23.030216>
- [16] A. David, P. T. Fini, K. W. Houser, Y. Ohno, M. P. Royer, K. A. G. Smet, M. Wei, and L. Whitehead, "Development of the IES method for evaluating the color rendition of light sources," *Opt. Express*, vol. 23, no. 12, p. 15888, 2015. <https://doi.org/10.1364/oe.23.015888>
- [17] A. Žukauskas, R. Vaicekauskas, P. Vitta, A. Tuzikas, A. Petrulis, and M. Shu, "Color rendition engine," *Opt. Express*, vol. 20, no. 5, p. 5356, 2012. <https://doi.org/10.1364/oe.20.005356>
- [18] M. S. Rea and J. P. FreyssinierNova, "Color rendering: A tale of two metrics," *Color Res. Appl.*, vol. 33, no. 3, pp. 192–202, 2008. <https://doi.org/10.1002/col.20399>
- [19] M. P. Royer, "Tutorial: Background and guidance for using the ANSI/IES TM-30 method for evaluating light source color rendition," *LEUKOS*, vol. 18, no. 2, pp. 191–231, 2021. <https://doi.org/10.1080/15502724.2020.1860771>
- [20] P. Cebrián, L. Pérez-Sienes, I. Sanz-Vicente, Á. López-Molinero, S. de Marcos, and J. Galbán, "Solving color reproducibility between digital devices: A robust approach of smartphones color management for chemical (bio)sensors," *Biosensors*, vol. 12, no. 5, p. 341, 2022. <https://doi.org/10.3390/bios12050341>
- [21] I. A. Vasilenko and L. N. Sinitsa, "Led-based Fourier transform absorption spectroscopy of HD17O in 13,165–14,060 cm⁻¹ spectral region," *J. Quant. Spectrosc. Radiat. Transfer*, vol. 324, p. 109067, 2024. <https://doi.org/10.1016/j.jqsrt.2024.109067>
- [22] P. Chiradeja and S. Yoomak, "Development of public lighting system with smart lighting control systems and internet of thing (IoT) technologies for smart city," *Energy Rep.*, vol. 10, pp. 3355–3372, 2023. <https://doi.org/10.1016/j.egy.2023.10.027>